Supplementary Information for

Boosting single-molecule fluorescence enhancement with Nanoaperture-nanoantenna hybrid system

Ting Chen[1‡], Zheyuan Zhu[1‡], Boyi Liu[1], Qiong He[1,2], Lei Zhou[1,2], and Yan-Wen Tan[1,2,3]*

[1]State Key Laboratory of Surface Physics and Department of Physics, Nano Photonic Structures (Ministry of Education), Fudan University, Shanghai 200433, China

[2]Shanghai Key Laboratory of Metasurfaces for Light Manipulation, Shanghai, 200433, China

[3]Multiscale Research Institute of Complex Systems, Fudan University, Shanghai 200433, China

‡ These authors contributed equally to this work.

* Corresponding Authors: Y.-W. Tan (ywtan@fudan.edu.cn),

Q.He. (qionghe@fudan.edu.cn) and

L.Zhou. (phzhou@fudan.edu.cn).

List of contents:

Section 1 – SEM pictures, structural parameters and far-field spectra of fabricated nano-systems

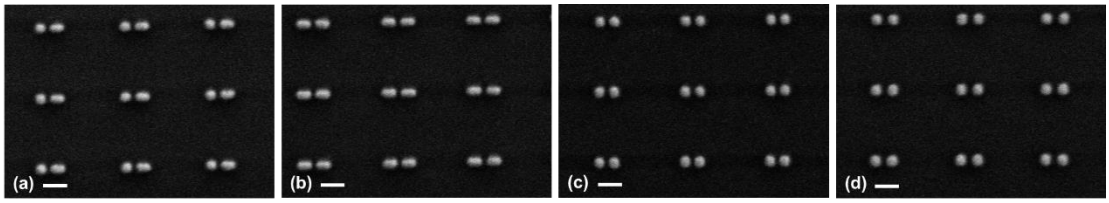

Figure S1. Scanning electron microscopy (SEM) images of the periodic array of nanoantennas fabricated via the first electron beam lithography. The corresponding bar lengths (b_1, b_2), gap (g), are: (a) $b_1 = 44\ nm\ b_2 = 60\ nm\ g = 20\ nm$; (b) $b_1 = 60\ nm\ b_2 = 60\ nm\ g = 20\ nm$; (c) $b_1 = 42\ nm\ b_2 = 42\ nm\ g = 20\ nm$; (d) $b_1 = 42\ nm\ b_2 = 42\ nm\ g = 30\ nm$, respectively. The shared nanoantenna periodic parameters of all nanoantennas are: $I_x = 360\ nm$ along the X-direction; $I_y = 300\ nm$ along the Y-direction. Scale bar: 100 nm.

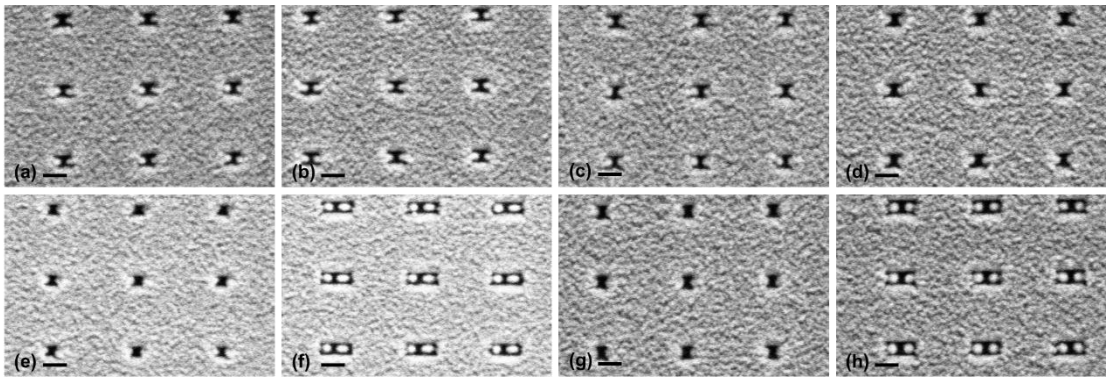

Figure S2. SEM images of the nanoaperture-nanoantenna hybrid systems fabricated via the second electron beam lithography. The corresponding bar lengths (b_1, b_2), gap (g), and nanoaperture length (L_H) are: (a) $b_1 = 44\ nm\ b_2 = 60\ nm\ g = 20\ nm\ L_H = 80\ nm$; (b) $b_1 = 60\ nm\ b_2 = 60\ nm\ g = 20\ nm\ L_H = 80\ nm$; (c) $b_1 = 42\ nm\ b_2 = 42\ nm\ g = 20\ nm\ L_H = 80\ nm$; (d) $b_1 = 42\ nm\ b_2 = 42\ nm\ g = 30\ nm\ L_H = 80\ nm$; (e) $b_1 = 44\ nm\ b_2 = 60\ nm\ g = 20\ nm\ L_H = 60\ nm$; (f) $b_1 = 40\ nm\ b_2 = 60\ nm\ g = 20\ nm\ L_H = 140\ nm$; (g) $b_1 = 42\ nm\ b_2 = 42\ nm\ g = 30\ nm\ L_H = 60\ nm$; (h) $b_1 = 42\ nm\ b_2 = 42\ nm\ g = 30\ nm\ L_H = 130\ nm$, respectively. The shared nanoantenna periodic parameters of all nano-systems are: $I_x = 360\ nm$ along the X-direction; $I_y = 300\ nm$ along the Y-direction. The shared nanoaperture width is: $W_H = 75\ nm$.Scale bar: 100 nm.

The geometrical parameters (shown in Table S1-S2, using the same abbreviated parameter names as in Figure 2a of the main text) of the nanoantennas and nanoapertures used in experimentally reported nano-systems were estimated according to SEM results (see Figs. S1-S2). In Table S1, b_1 (b_2) and w_{b1} (w_{b2}) are the lengths and width of bar 1 (bar 2), respectively; g denotes the gap between the two bars; I_x and I_y define the periodicity of the nanoantenna array in the X and Y directions, respectively. In Table S2, L_H and W_H represent the nanoaperture length and width; Δ_x and Δ_y indicate the offset of the nanoaperture relative to the nanoantenna in the X and Y directions, respectively. We acquired the transmission spectra of the nano-systems using the approach described in the Material and methods section of the main text. As shown in Figure S4, variations in the nanoaperture lengths exhibit only minor influence on the transmission spectra of the nano-systems. With the nanoaperture length increase, the nanoantenna transitions from being mostly embedded in PMMA (n = 1.49) to being fully exposed in water (n = 1.33). This change in the refractive index of surrounding dielectric environment induces a slight blue shift in the resonance peak of the nano-systems' transmission spectrum and a small increase in the minimum transmittance.

Table S1: Measured geometrical parameters of nanoantennas based on SEM image

Sample No: **Design value**	b_1 **(nm)**	b_2 **(nm)**	w_{b1} **(nm)**	w_{b2} **(nm)**	g **(nm)**	I_x **(nm)**	I_y **(nm)**
1. $b_1 = 40$ $b_2 = 60$							
$w_{b1} = 39$ $w_{b2} = 33$	43.40	59.81	38.64	35.12	21.23	362.96	295.22
$g = 20$	±1.25	±0.93	±1.64	±1.49	±1.28	±1.66	±1.54
$I_x = 360$ $I_y = 300$							
2. $b_1 = 60$ $b_2 = 60$							
$w_{b1} = 33$ $w_{b2} = 33$	62.48	62.71	35.88	35.69	20.90	363.21	298.38
$g = 20$	±1.68	±1.84	±1.51	±2.83	±2.23	±2.29	±3.53
$I_x = 360$ $I_y = 300$							
3. $b_1 = 40$ $b_2 = 40$							
$w_{b1} = 42$ $w_{b2} = 42$	40.65	41.79	44.57	44.60	22.44	363.16	299.23
$g = 20$	±1.66	±2.21	±2.47	±1.89	±1.79	±1.57	±2.31
$I_x = 360$ $I_y = 300$							

4. $b_1 = 40\ b_2 = 40$ $w_{b1} = 42\ w_{b2} = 42$ $g = 30$ $I_x = 360\ I_y = 300$	41.75 ±1.94	42.47 ±2.01	43.43 ±2.56	44.07 ±2.63	30.83 ±1.54	363.20 ±2.77	298.98 ±2.72

Table S2: Measured geometrical parameters of nanoapertures based on SEM images

Sample No: Design value	L_H (nm)	W_H (nm)	Δ_x (nm)	Δ_y (nm)
1. $b_1 = 40\ b_2 = 60\ w_{b1} = 39\ w_{b2} = 33$ $g = 20\ I_x = 360\ I_y = 300$ $L_H = 80\ W_H = 75$	72.85 ±2.42	52.12 ±1.43	2.02 ±0.13	4.33 ±1.81
2. $b_1 = 60\ b_2 = 60\ w_{b1} = 33\ w_{b2} = 33$ $g = 20\ I_x = 360\ I_y = 300$ $L_H = 80\ W_H = 75$	72.15 ±1.74	52.17 ±1.37	1.93 ±0.08	1.62 ±2.16
3. $b_1 = 40\ b_2 = 40\ w_{b1} = 42\ w_{b2} = 42$ $g = 20\ I_x = 360\ I_y = 300$ $L_H = 80\ W_H = 75$	68.96 ±2.16	53.91 ±1.11	-0.65 ±2.24	1.64 ±1.67
4. $b_1 = 40\ b_2 = 40\ w_{b1} = 42\ w_{b2} = 42$ $g = 30\ I_x = 360\ I_y = 300$ $L_H = 80\ W_H = 75$	70.40 ±1.37	54.31 ±1.49	1.97 ±0.12	1.59 ±1.10
5. $b_1 = 40\ b_2 = 60\ w_{b1} = 39\ w_{b2} = 33$ $g = 20\ I_x = 360\ I_y = 300$ $L_H = 60\ W_H = 75$	45.79 ±2.51	42.30 ±1.30	1.89 ±0.14	-0.57 ±2.02
6. $b_1 = 40\ b_2 = 60\ w_{b1} = 39\ w_{b2} = 33$ $g = 20\ I_x = 360\ I_y = 300$ $L_H = 140\ W_H = 75$	134.73 ±1.80	48.23 ±0.74	2.03 ±0.04	-0.75 ±0.93
7. $b_1 = 40\ b_2 = 40\ w_{b1} = 42\ w_{b2} = 42$ $g = 30\ I_x = 360\ I_y = 300$ $L_H = 60\ W_H = 75$	53.46 ±2.67	54.71 ±1.08	2.09 ±0.10	2.04 ±1.21
8. $b_1 = 40\ b_2 = 40\ w_{b1} = 42\ w_{b2} = 42$ $g = 30\ I_x = 360\ I_y = 300$ $L_H = 130\ W_H = 75$	123.22 ±2.34	56.35 ±1.08	2.01 ±0.08	2.42 ±1.00

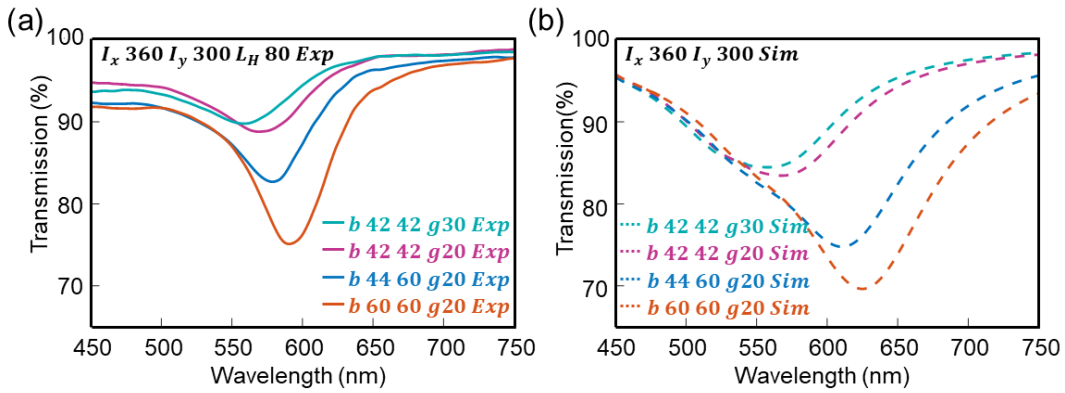

Figure S3. Experimental (a) and simulated (b) transmission spectra of nanoaperture-nanoantenna hybrid systems with various nanoantenna configurations. All systems have a fixed nanoaperture length ($L_H = 80\ nm$) and nanoantenna periods ($I_x = 360\ nm\ I_y = 300\ nm$). Curves correspond to the following configurations: $b_1 = 42\ nm\ b_2 = 42\ nm\ g = 30\ nm$ (cyan); $b_1 = 42\ nm\ b_2 = 42\ nm\ g = 20\ nm$ (purple); $b_1 = 44\ nm\ b_2 = 60\ nm\ g = 20\ nm$ (blue); $b_1 = 60\ nm\ b_2 = 60\ nm\ g = 20\ nm$ (orange).

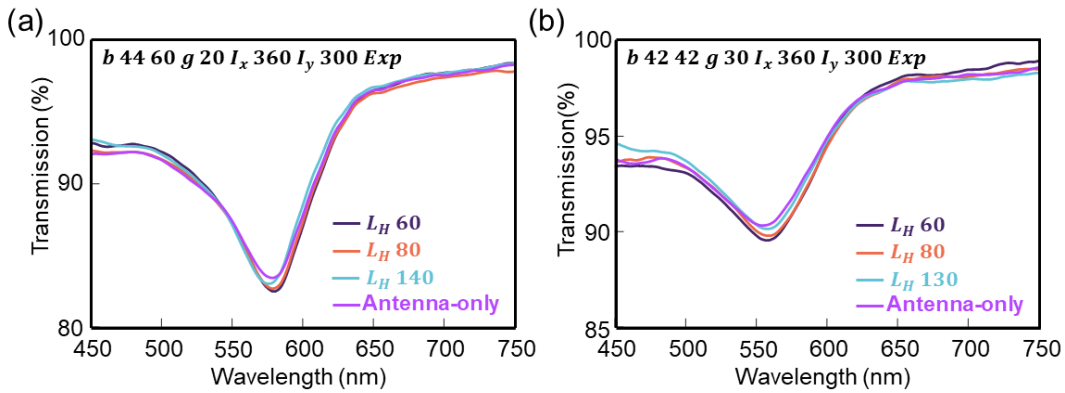

Figure S4. Transmission spectra of nanoantenna-only systems and nanoaperture-nanoantenna hybrid systems with varying nanoaperture lengths (L_H). (a) Experimentally measured spectra for nano-systems with fixed nanoantenna period ($I_x = 360\ nm\ I_y = 300\ nm$) and nanoantenna configuration ($b_1 = 40\ nm\ b_2 = 60\ nm\ g = 20\ nm$). (b) Experimentally measured spectra for nano-systems with the same fixed period but a different nanoantenna configuration ($b_1 = 40\ nm\ b_2 = 40\ nm\ g = 30\ nm$). Curves correspond to the following: hybrid systems $L_H = 60\ nm$ (black); $L_H = 80\ nm$ (red); $L_H = 140/130\ nm$ (cyan), nanoantenna-only system (purple).

Section 2 – Fluorescence intensity distributions of the glass reference groups

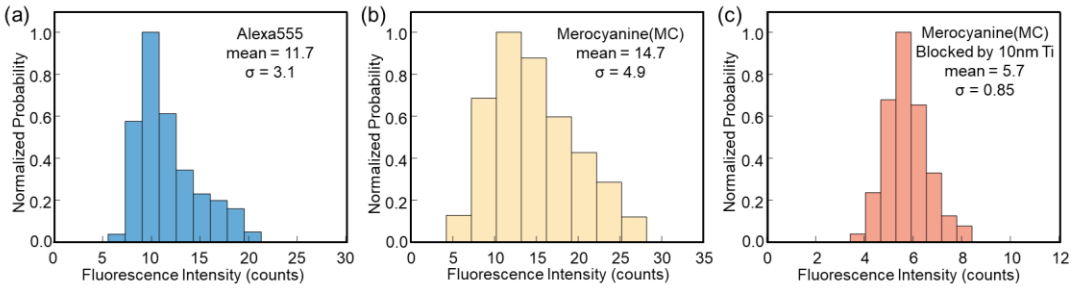

Figure S5. Fluorescence intensity histogram plot for the glass reference groups. (a) Distribution from 125 pM Alexa555 in 10 mM HEPES + 0.5% Triton X-100 buffer (pH 7.5, HEPES-TX buffer) incubated on bare glass substrates. (b) Distribution from 1 μM Spiropyran (SP) + Merocyanine (MC) in HEPES-TX buffer incubated on bare glass substrates. (c) Distribution from 10 μM SP+MC in HEPES-TX buffer incubated on glass substrates spin-coated with 75-nm PMMA and vapor-deposited with a 10-nm titanium (Ti) layer by oblique-angle electron-beam evaporation. Each distribution comprises 1000 individual fluorescent molecules. In (b) and (c), a statistically significant 61% reduction in MC molecule fluorescence intensity was observed under signal shielding by the 10-nm Ti layer.

Section 3 –Supplementary figures for "Fluorescence enhancement by a typical hybrid system" section

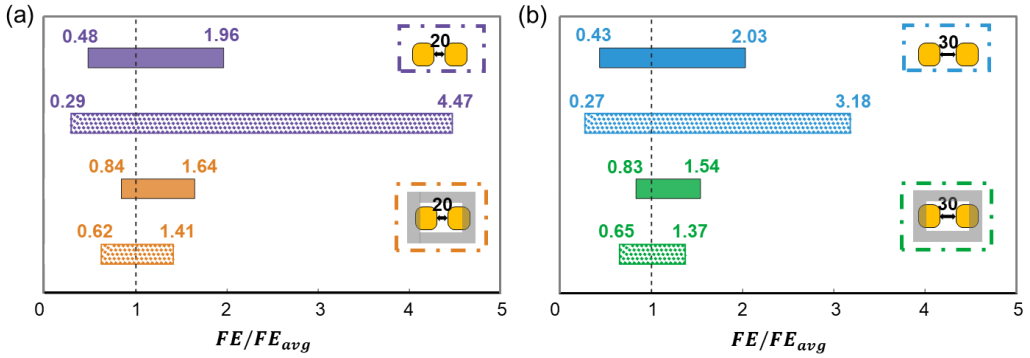

Figure S6. Relative distribution widths (W_{rel}s) for Alexa555-optimized nano-systems, calculated using Equation (3) in the main text. (a) W_{rel}s for nano-systems with $g = 20\,nm$. Purple/orange: nanoantenna-only/hybrid systems. Fill/dot: W_{rel}s of experimental/simulated distributions. (b) W_{rel}s for nano-systems with $g = 30\,nm$. Blue/green: nanoantenna-only/hybrid systems. Fill/dot: W_{rel}s of experimental/simulated distributions.

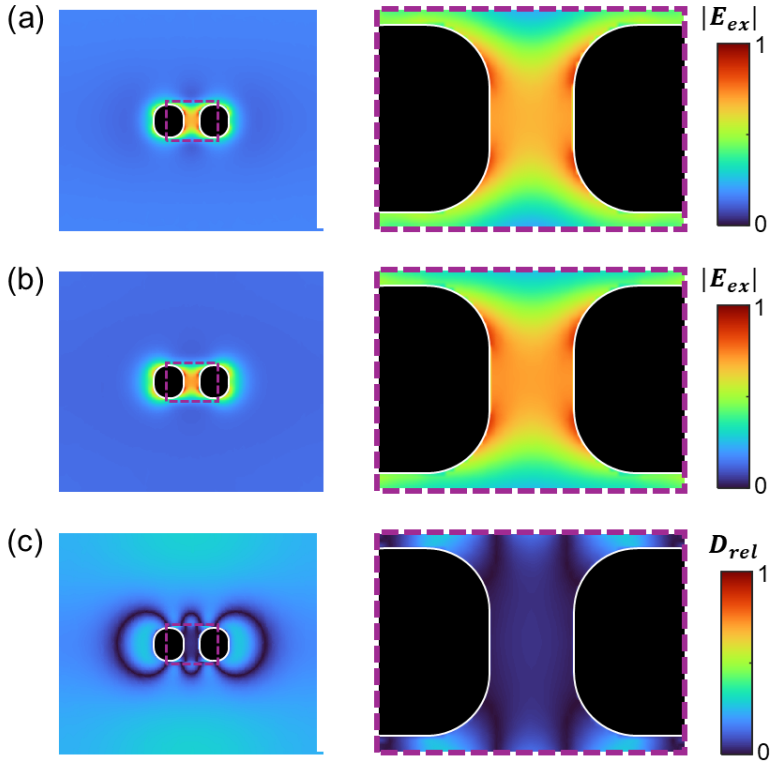

Figure S7. Numerical simulation results of excitation field distributions on the plane parallel to the substrate. (a) Hybrid system excitation field. (b) Nanoantenna-only system excitation field. (c) Relative difference distribution $D_{rel} = ||E_{ex,hyb}| - |E_{ex,ao}||/|E_{ex,ao}|$ derived from (a) and (b), where $|E_{ex,hyb}|$ and $|E_{ex,hyb}|$ denote the electric field magnitudes at identical positions for hybrid and nanoantenna-only systems, respectively. Left panels in all subfigures display field distributions or D_{rel} across the full periodic nanostructure ($I_x = 360$ nm, $I_y = 300$ nm), with a centered 70 nm × 50 nm region outlined by purple dashed boxes. Right panels show magnified views of these central regions. All simulations correspond to the planes of maximum fluorescence enhancement for the nanoantenna, using the symmetric $g = 20\,nm$ structure employed in Alexa555 fluorescence enhancement experiment in the main text.

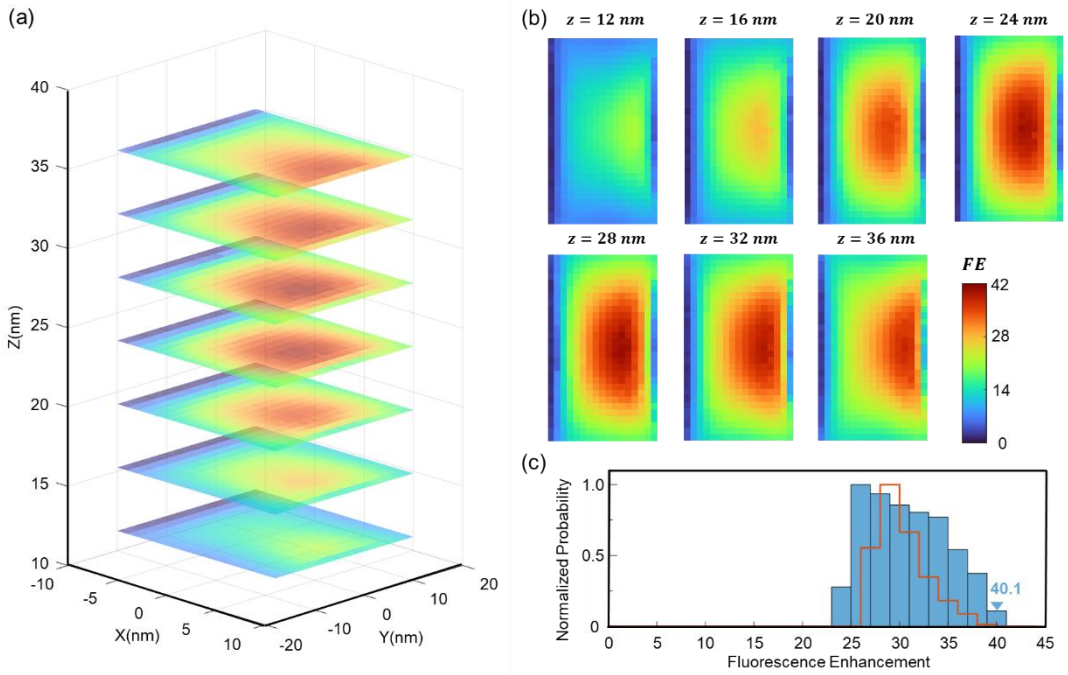

Figure S8. Fluorescence enhancement distributions on multiple planes within the gap region of asymmetric nanoantenna. (a) Spatial positions of the seven simulated planes within the gap region (z = 12, 16, 20, 24, 28, 32, 36 nm). The x-, y-, and z-axes correspond to the nanoantenna's long axis, short axis, and substrate normal direction, respectively. (b) Fluorescence enhancement distribution on each individual plane. (c) 3D fluorescence enhancement distribution (blue bars) generated by integrating hotspot region data from multiple planes in (b), compared with the experimental distribution of the nanoaperture-nanoantenna hybrid system with symmetric nanoantenna configurations (orange outline) in Figure 4a of the main text. Simulations used the asymmetric nanoantenna employed in the merocyanine fluorescence enhancement experiments described in the main text.

Section 4 – Numerical simulations of the excitation/emission processes and the fluorescence enhancement factor

Figure 3e was simulated using the finite element method (FEM) implemented in COMSOL Multiphysics software. Compared with the nanoantenna-only system, the hybrid system features a 10 nm thick titanium (Ti) layer, positioned 75 nm to 85 nm away from the glass substrate. The optical constants for the Ti layer are sourced from the Johnson and Christy (1974) database. The region between the glass substrate and the Ti layer is filled with PMMA, which is modeled as a dielectric with a relative permittivity of $\varepsilon_{pmma} = 1.49^2$. For the excitation process at the wavelength of 532 nm, the system was illuminated from below by a plane wave propagating in the +z direction (substrate normal direction), with its electric field polarized along the x-axis (nanoantenna's long axis). For the emission process, an x-oriented electric dipole source at the wavelength of 568 nm was introduced. Specifically, in the nanoantenna-only system, the dipole was positioned 20 nm from the left side of the structure and 24 nm above the glass substrate. Conversely, in the hybrid system, the dipole was placed at the same x-coordinate but was located 10 nm above the upper surface of the Ti layer.

By applying a similar approach, the spatial fluorescence enhancement distributions shown in Figures 3g and 4c were generated by iteratively placing the dipole at different positions and performing the corresponding theoretical calculations. The theoretical foundation for this procedure is detailed below.

In simulations of single molecule fluorescence, the fluorescence enhancement factor is the product of the enhancement factors of the excitation rate and quantum yield. Therefore, the fluorescence enhancement factor can be expressed as:

$$FE = F_{ex} \times F_{em} \qquad (S1)$$

where $F_{ex} \equiv \gamma_{ex}/\gamma_{ex}^0$ and $F_{em} \equiv q/q^0$, with γ_{ex} and q denoting the excitation rate and quantum yield of the molecule in the presence of a nano-antenna placed nearby, while those with superscript "0" represent their free-space counterparts.

The excitation rate of a molecule γ_{ex} is proportional to:

$$\gamma_{ex} \sim |\boldsymbol{E}_{loc} \times \boldsymbol{p}_{ex}|^2 \tag{S2}$$

where $\boldsymbol{E}_{loc}$ denotes the local electric field experienced by the molecule and $\boldsymbol{p}_{ex}$ is the molecule's transition dipole moment at the excitation frequency. Since dipole misalignment with the electric field sharply reduces excitation rate, submerging fluorescence signals in background noise, our simulation approximates by focusing solely on parallel alignments. Furthermore, as an intrinsic property of a molecule, $\boldsymbol{p}_{ex}$ is essentially constant and independent of the presence of a nano-antenna, and hence the enhancement of excitation rate F_{ex} simplifies to:

$$F_{ex} = \frac{\gamma_{ex}}{\gamma_{ex}^0} = \frac{|\boldsymbol{E_{loc}}|^2}{|\boldsymbol{E_0}|^2} \tag{S3}$$

where $\boldsymbol{E_0}$ is the electric field at the molecule's position without a nearby nano-antenna, under identical external illumination.

The quantum yield of a molecule is defined as:

$$q = \frac{\Gamma_{em}^r}{\Gamma_{em}^r + \Gamma_{em}^{nr}} \tag{S4}$$

where Γ_{em}^r and Γ_{em}^{nr} denote the radiative and nonradiative decay rates of the entire system, respectively. The total nonradiative decay rate can then be rewritten as:

$$\Gamma_{em}^{nr} = \Gamma_{em}^i + \gamma_{em}^{nr} \tag{S5}$$

which contains the absorptions contributed by the nano-antenna (Γ_{em}^i) and the molecule (γ_{em}^{nr}).

Since direct simulation of molecular absorption is infeasible, and assuming the antenna does not alter the molecule's intrinsic nonradiative decay rate, we express it in terms of the free-space quantum yield (q^0) and free-space radiative decay rate (γ_{em}^r) as:

$$\gamma_{em}^{nr} = \gamma_{em}^r \frac{1-q^0}{q^0} \tag{S6}$$

Hence, the enhancement of quantum yield F_{em} is:

$$F_{em} = \frac{q}{q^0} = \frac{1}{q^0} \frac{\frac{\Gamma_{em}^r}{\gamma_{em}^r}}{\frac{\Gamma_{em}^r}{\gamma_{em}^r} + \frac{\Gamma_{em}^i}{\gamma_{em}^r} + \frac{1-q^0}{q^0}} \tag{S7}$$

Equation $(S3)$ and $(S7)$ can be evaluated in simulations. Specifically, the local electric field in Equation $(S3)$ is computed directly from electromagnetic simulations at the excitation wavelength of 532 nm. For Equation $(S7)$, simulations are performed at the emission wavelengths of 568 nm for Alexa555 molecules and 612 nm for MC molecules. The radiative decay rate Γ_{em}^r, is determined by integrating outward the power flow across enclosing surfaces (P_{out}) in the simulation domain, while the antenna-induced absorption rate Γ_{em}^i is obtained by integrating the power loss (Q_{loss}) within the nano-antenna volume. These rates are normalized using the following relations:

$$\frac{\Gamma_{em}^r}{\gamma_{em}^r} = \frac{P_{out}}{P_{out}^0} \tag{S8}$$

$$\frac{\Gamma_{em}^i}{\gamma_{em}^r} = \frac{Q_{loss}}{P_{out}^0} \tag{S9}$$

where P_{out}^0 represents the free-space radiation power of the corresponding dipole.

Based on the theoretical methodology, we performed detailed simulations for the plane that yields the maximum fluorescence enhancement. In the excitation simulation, the simulated electric field was sampled at a 2 nm interval within a 10 nm region surrounding the structures and at a finer 1 nm interval within the central 28 nm × 28 nm square area. For the subsequent emission simulation, we modeled the fluorescence molecule as an electric dipole. This dipole was placed individually at each coordinate where the electric field had been previously sampled, and the simulation was run iteratively to cover all specified points.

Section 5 – Properties of merocyanine

5.1. Spiropyran- Merocyanine photoisomerization

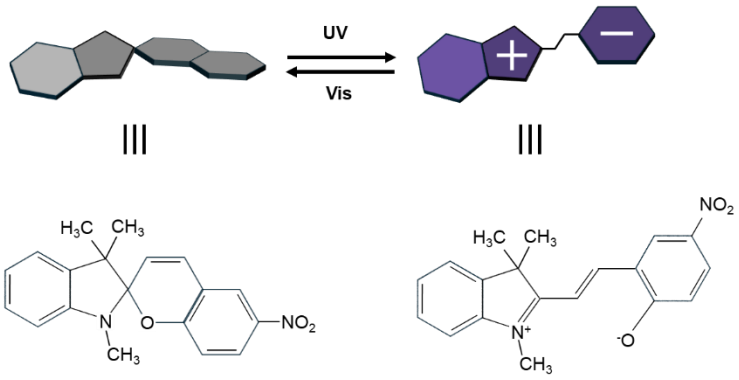

Figure S9. Schematics and chemical structures of reversible photoisomerization between spiropyran (SP) and merocyanine (MC).

Spiropyran (SP) molecules can undergo photoisomerization to form excitable Merocyanine (MC) molecules upon exposure to UV light. Conversely, MC molecules can revert back to SP molecules upon exposure to visible light.

5.2. Evaluation of quantum yield of merocyanine

To measure the quantum yield of Merocyanine (Sigma-Aldrich) in 10 mM HEPES + 0.5% Triton X-100 solutions (pH 7.5, HEPES-TX solution), Atto550 (Sigma-Aldrich) was used as the quantum yield standard reference. We diluted both dyes to appropriate concentrations such that their absorption peaks were below 0.2 OD, ensuring negligible self-absorption effects along the fluorescence path.[1] The Spiropyran (SP) and Merocyanine (MC) molecules were diluted to two concentrations (20 μM SP + MC and 2 μM SP + MC) to verify the absence of aggregation-caused quenching effects at the 20 μM SP + MC concentration used in our fluorescence experiment. The quantum yield ϕ is defined as the ratio of emitted photons to the absorbed photons. Assuming that the emission of the dye molecules is isotropic and their quantum yield is independent of the excitation wavelength, then the integrated area of their emission spectrum can approximately represent the intensity of fluorescence (see Figure S10). Taking into account the solvent's refractive index and the absorbance of the dye molecule at the

excitation wavelength, the quantum yield ϕ can be expressed by the following formula:[2]

$$\phi_{sam} = \frac{F_{sam} n_{sam}^2}{F_{ref} \cdot n_{ref}^2} \times \frac{I_{ref}[1 - 10^{-A_{ref}}]}{I_{sam}[1 - 10^{-A_{sam}}]} \times \phi_{ref} \qquad (S10)$$

Where F is the integrated fluorescence intensities, n is the refractive indexes of solvents. I is the excitation intensity and A is the absorbance of solution. Parameters with the subscript ' ref ' or ' sam ' denote those corresponding to the standard reference or measured sample, respectively. Because the sample and reference standard were measured using the same spectrometer and identical measurement parameters, the excitation intensity was identical for both ($I_{ref} = I_{sam}$). Consequently, the corresponding terms could be cancelled out in the formula. ϕ_{ref} is the quantum yield of 150 nM Atto550 in 10 mM HEPES solution (pH 7.5) at room temperature. Prior to MC molecules' emission spectrum measurement, the sample was irradiated for 15 minutes with a 40 mW, 340 nm UV lamp to maximize SP-to-MC photoconversion. After the emission spectrum measurement was completed, the sample received another irradiation for 6 minutes using the same UV lamp to maintain the concentration of MC molecules, followed by the subsequent absorption spectrum measurement. Parameters used in calculation and ϕ_{sam} of MC are shown in Table S3.

Table S3: Parameters of Atto550 and Merocyanine. Where F represents the integrated fluorescence intensity over the whole spectrum, A is the absorbance of solution, and n denotes refractive indexes.

	F	A@532nm	n of solvents	ϕ
Atto550 (150nM)	81689.26	0.006703	1.3330	0.8000
MC (20μM SP + MC)	113486.30	0.080473	1.3337	0.1007
MC (2μM SP + MC)	16557.71	0.011163	1.3337	0.0980

The quantum yields of MC molecules were both approximately 10% at two sample concentrations, indicating that aggregation-induced quenching did not occur at the MC concentration used in our fluorescence observation experiments.

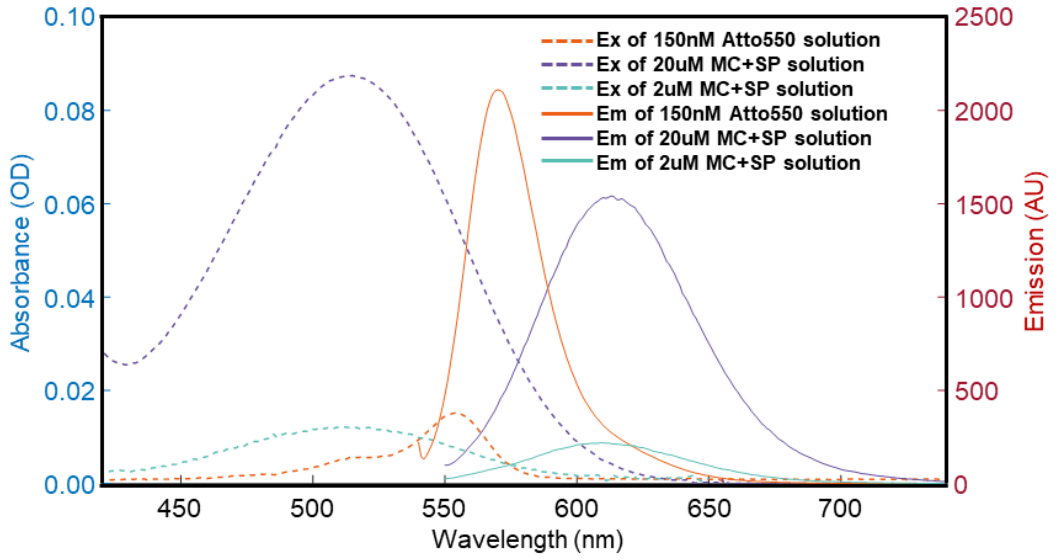

Figure S10. Absorption spectra of: (dashed-orange line) 150 nM Atto550 in 10 mM HEPES solution (pH 7.5, HEPES solution); (dashed-purple line) 20 μM SP + MC in 10 mM HEPES + 0.5% Triton X-100 solutions (pH 7.5, HEPES-TX solution); (dashed-cyan line) 2 μM SP + MC in HEPES-TX solution; Emission spectra of same solutions of: (solid-orange line) 150 nM Atto550 in HEPES solution; (solid-purple line) 20 μM SP + MC in HEPES-TX solution; (soild-cyan line) 2 μM SP + MC in HEPES-TX solution.

5.3. Evaluation of approximate concentration of merocyanine under experimental conditions

MC and SP exist in a dynamic equilibrium in solution. To verify this equilibrium, a 20 μM SP + MC in 10 mM HEPES + 0.5% Triton X-100 buffer solution (pH 7.5) was irradiated for 15 minutes using a 40 mW, 340 nm UV lamp to maximize SP-to-MC photoconversion. Subsequently, this solution was irradiated using the 532 nm emission line from the spectrometer's xenon lamp (Hitachi, F-2500). The emission spectrum of the solution was measured at 0, 5, 10, 15, and 20 minutes after the start of xenon lamp irradiation. We observed that the emission intensity from MC in the solution decayed single-exponentially with increasing xenon lamp irradiation time (see Figure S11), eventually decreasing to one-fifth of its initial intensity. This indicates that a significant concentration of MC persisted in the solution under xenon lamp irradiation, rather than being completely converted back to SP, demonstrating the existence of the dynamic

equilibrium between SP and MC. After irradiating with the xenon lamp for 20 minutes, the solution was placed in the dark for 10 minutes. Upon remeasuring the emission spectrum, we found that the emission intensity at the 612 nm peak increased from 309 au (after 20 min irradiation) to 587 au. This recovery in MC concentration indicates that SP molecules can spontaneously convert back to MC molecules in the dark.

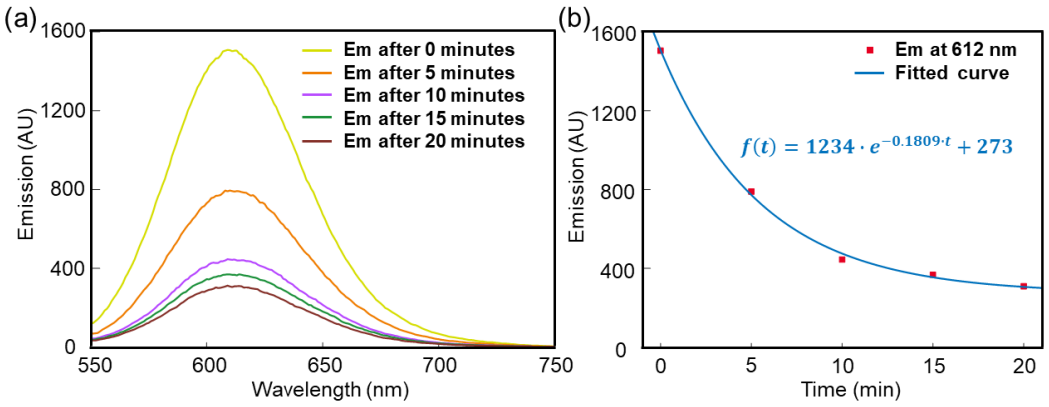

Figure S11. Decrease in emission intensity of 20 μM SP + MC solution with increasing irradiation time by the spectrometer's xenon lamp. (a) Emission spectra of the 20 μM SP + MC in 10 mM HEPES + 0.5% Triton X-100 solutions (pH 7.5) after 0 min (lemon yellow), 5 min (orange), 10 min (purple), 15 min (green), and 20 min (brown) of xenon lamp irradiation. (b) Emission intensity at the 612 nm peak position extracted from the emission spectra, plotted as a function of xenon lamp irradiation time. The spectral data are represented by red square markers, and the fitted curve is shown as a blue line.

Notably, although the concentration of MC + SP in our sample solution was several orders of magnitude higher than that of Atto550 in the reference standard, only a small fraction of the SP molecules was converted to MC molecules upon irradiation with the 340 nm UV lamp. Given that the molar extinction coefficients of the MC molecule and the Atto550 molecule at their respective maximum absorption wavelengths are comparable ($\sim 10^5\ L \cdot M^{-1} \cdot cm^{-1}\ vs.\ 1.2 \times 10^5\ L \cdot M^{-1} \cdot cm^{-1}$), we can estimate, based on their absorbances at these wavelengths, that the concentration of MC molecules in the 20 μM MC+SP sample solution is approximately 1 μM. When the SP + MC solution is irradiated with 532 nm laser, the actual concentration of MC rapidly decreases until reaching an equilibrium state. This equilibrium concentration of MC is

dependent on the intensity of the laser. To estimate the concentration of MC molecules in the incubation solution (20 μM SP + MC) during fluorescence observation experiments under irradiation by the 532 nm laser, we prepared the incubation solution and placed it in the microscope excitation light path. It was irradiated with the 532 nm laser for 3 minutes (twice the duration of our fluorescence observation period, ensuring the MC concentration reached dynamic equilibrium). The solution was then placed in the dark and transferred to the spectrometer for emission spectrum measurement (see Figure S12). By calculating the ratio of the integrated areas of the excitation spectra before and after 532 nm laser irradiation (after background subtraction), we determined that the post-irradiation concentration of MC was only 3.82% of the pre-irradiation value, approximately 38 nM. If we account for the gradual reversion of SP molecules back to MC molecules in the dark environment during the transfer of incubation solution to spectrometer, the actual post-irradiation concentration of MC was even lower than 38 nM.

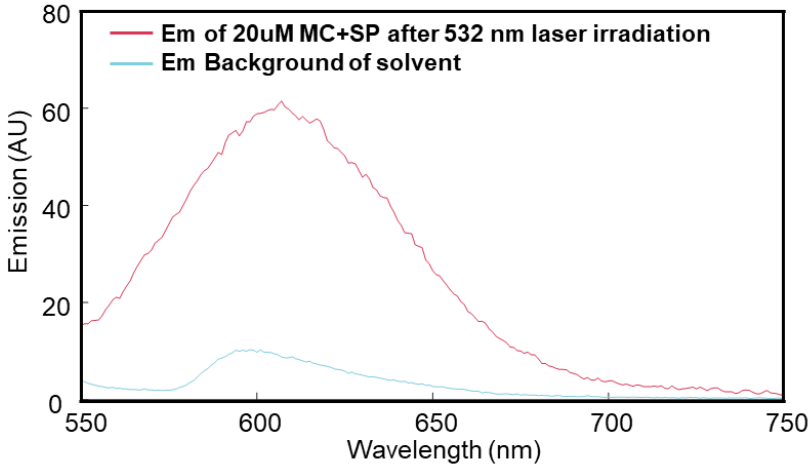

Figure S12. Emission spectra of: (solid-orange line) 20 μM SP + MC in 10 mM HEPES + 0.5% Triton X-100 solution after 532 nm laser irradiation; (solid-cyan line) Background of 10 mM HEPES + 0.5% Triton X-100 solvent.

Section 6 – Supplementary figures for "Influences of Asymmetry of Nanoantenna Design on FE Performance" section

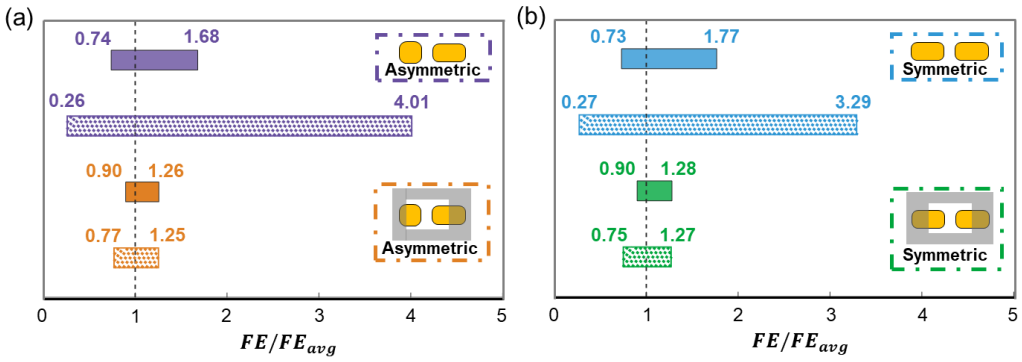

Figure S13. Relative distribution widths (W_{rel} s) for merocyanine-optimized nano-systems, calculated using Equation (3) in the main text. (a) W_{rel}s for nano-systems with asymmetric configuration. Purple/orange: nanoantenna-only/hybrid systems. Fill/dot: W_{rel} s of experimental/simulated distributions. (b) W_{rel}s for nano-systems with symmetric configuration. Blue/green: nanoantenna-only/hybrid systems. Fill/dot: W_{rel} s of experimental/simulated distributions.

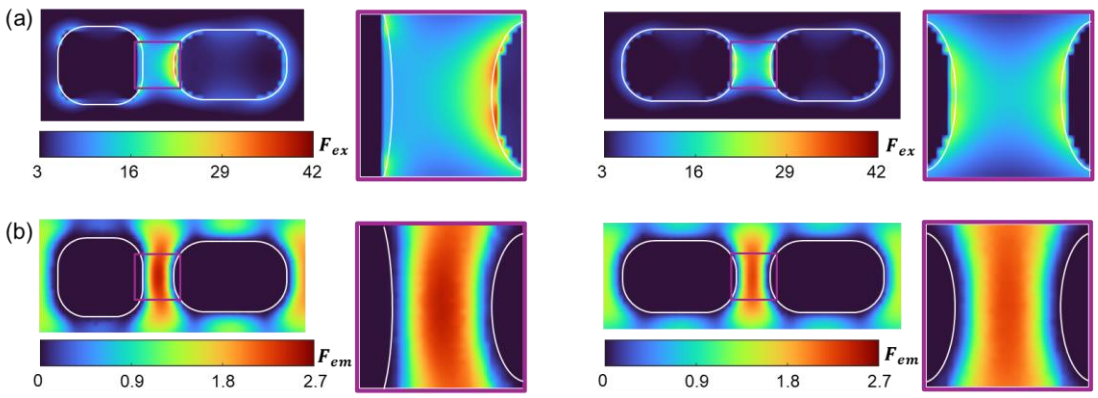

Figure S14. Numerical simulations of excitation rate enhancement (F_{ex} , (a)) and quantum yield enhancement (F_{em} , (b)) distributions on the plane parallel to the substrate for asymmetric (left) and symmetric (right) nanoantennas. The left panels display enhancement maps across the entire nanoantenna structure, with the gap region outlined in purple. The right panels provide magnified views of this highlighted gap region. The simulation planes are located at the nanoantennas' maximum fluorescence enhancement planes.

Section 7 – Steady state distribution of molecules

In our model, the spatial distribution of molecules is governed by the interplay between thermal diffusion and external field forces.[3] The total molecular flux J comprises two distinct components:

$$\boldsymbol{J} = \boldsymbol{J}_{diff} + \boldsymbol{J}_{drift} \tag{S11}$$

where the diffusive flux $\boldsymbol{J}_{diff}$ follows Fick's law:

$$\boldsymbol{J}_{diff} = -D\nabla c \tag{S12}$$

and the drift flux $\boldsymbol{J}_{drift}$ is given by:

$$\boldsymbol{J}_{drift} = c\boldsymbol{v} \tag{S13}$$

Here, D denotes the diffusion coefficient, c represents the density of molecules, and $\boldsymbol{v}$ is the drift velocity induced by external forces.

Under the influence of external forces, molecules reach a terminal drift velocity due to viscous drag from the surrounding medium. At equilibrium, when the external force balances the damping force (i.e., $\boldsymbol{F}_{ext} + \boldsymbol{F}_{damp} = 0$), the drift velocity becomes proportional to the external force. Consequently, the drift flux can be expressed as:

$$\boldsymbol{J}_{drift} = \mu \boldsymbol{F}_{ext} c \tag{S14}$$

where μ is the molecular mobility, related to the diffusion coefficient through the Einstein relation:

$$\mu = \frac{D}{k_B T} \tag{S15}$$

with k_B being Boltzmann's constant and T the absolute temperature.

The conservation of molecular numbers requires that the flux satisfies the continuity equation:

$$\frac{\partial c}{\partial t} = -\nabla \cdot \boldsymbol{J} = D\nabla^2 c - \nabla \cdot (\mu \boldsymbol{F}_{ext} c) \tag{S16}$$

At steady state, where $\partial c/\partial t = 0$, this equation reduces to:

$$\nabla \cdot \left[D \left(\nabla c - \frac{c}{k_B T} \boldsymbol{F}_{ext} \right) \right] = 0 \tag{S17}$$

For spatially uniform diffusion coefficient and temperature, this simplifies to:

$$\frac{\nabla c}{c} = \frac{\boldsymbol{F}_{ext}}{k_B T} \tag{S18}$$

For conservative forces, such as those arising from electric fields, the force can be expressed as the negative gradient of a potential energy U:

$$\boldsymbol{F}_{ext} = -\nabla U \tag{S19}$$

Substituting this into Equation (S18) yields:

$$\frac{\nabla c}{c} = -\frac{\nabla U}{k_B T} \tag{S20}$$

Integration of this equation gives the Boltzmann distribution:

$$c(\boldsymbol{r}) = c_0 \exp\left(-\frac{U(\boldsymbol{r})}{k_B T} \right) \tag{S21}$$

where c_0 is normalization constant.

To determine the potential energy in an electric field, we employ the Lorentz oscillator model, treating each molecule as an induced electric dipole. The equation of motion for bound electrons under an applied electric field $\boldsymbol{E}(t)$ is:

$$m \frac{d^2 \boldsymbol{r}}{dt^2} + m\gamma \frac{d\boldsymbol{r}}{dt} + m\omega_0^2 \boldsymbol{r} = -e\boldsymbol{E}(t) \tag{S22}$$

where m is the electron mass, e is the elementary charge, γ is the damping coefficient, and ω_0 is the natural oscillation frequency. Solving in the frequency domain (i.e., $d/dt \rightarrow -i\omega$), we obtain:

$$-m\omega^2 \boldsymbol{r} - im\omega\gamma \boldsymbol{r} + m\omega_0^2 \boldsymbol{r} = -e\boldsymbol{E}(\omega) \tag{S23}$$

Solving the displacement:

$$\boldsymbol{r} = -\frac{e}{m}\frac{1}{\omega_0^2 - \omega^2 - i\omega\gamma}\boldsymbol{E}(\omega) \tag{S24}$$

The induced dipole moment $\boldsymbol{p} = -e\boldsymbol{r}$ defines the molecular polarizability α:[4]

$$\boldsymbol{p} = \alpha\boldsymbol{E} \tag{S25}$$

$$\alpha = \frac{e^2}{m}\frac{1}{(\omega_0^2 - \omega^2) - i\omega\gamma} \tag{S26}$$

The time-averaged potential energy of an induced dipole in an electric field is:

$$U(\boldsymbol{r}) = -\frac{1}{2}\mathrm{Re}[\alpha]|\boldsymbol{E}(\boldsymbol{r})|^2 \tag{S27}$$

Substituting this into the Boltzmann distribution (Equation (S21)), we obtain the final expression for the steady-state molecular distribution:

$$c(\boldsymbol{r}) = c_0 \exp\left(\frac{\mathrm{Re}[\alpha]}{2k_B T}|\boldsymbol{E}(\boldsymbol{r})|^2\right) \tag{S28}$$

This result demonstrates that molecules accumulate in regions of low electric field intensity when $\mathrm{Re}[\alpha] < 0$, corresponding to excitation frequencies above the resonance frequency of the molecules ($\omega > \omega_0$).[5]

Section 8 – Factors influencing the optimal nanoaperture size

For the molecular distribution in the steady-state region, normalization can be achieved using the background molecular density in the solution:

$$\frac{c(\boldsymbol{r})}{c_{bg}} = \exp\left[\frac{\mathrm{Re}[\alpha]}{2k_B T}\left|\boldsymbol{E}_{bg}\right|^2\left(\frac{|\boldsymbol{E}(\boldsymbol{r})|^2}{\left|\boldsymbol{E}_{bg}\right|^2} - 1\right)\right] \quad (S29)$$

For simplicity, we define the dimensionless factor $-\eta$ as $\frac{\mathrm{Re}[\alpha]}{2k_B T}\left|E_{bg}\right|^2$. Substituting this into equation (S29) yields:

$$c(\boldsymbol{r})/c_{bg} = \exp\left[-\eta\left(\frac{|E(\boldsymbol{r})|^2}{\left|E_{bg}\right|^2} - 1\right)\right] \quad (S30)$$

For larger values of η (indicating higher polarizability, stronger incident field, and lower temperature), the electric field exerts a dominant influence on molecular behavior. In this scenario, a larger nanoaperture size is required to ensure that sufficient molecules can pass through the nanoaperture while being shielded from the edge effects of the electric field. Conversely, for smaller values of η (indicating lower polarizability, weaker incident field, and higher temperature), thermal diffusion governs the molecular movement. Here, molecules can traverse the nanoaperture more readily, allowing a smaller nanoaperture size to suffice and enabling primary excitation within the hotspot region.

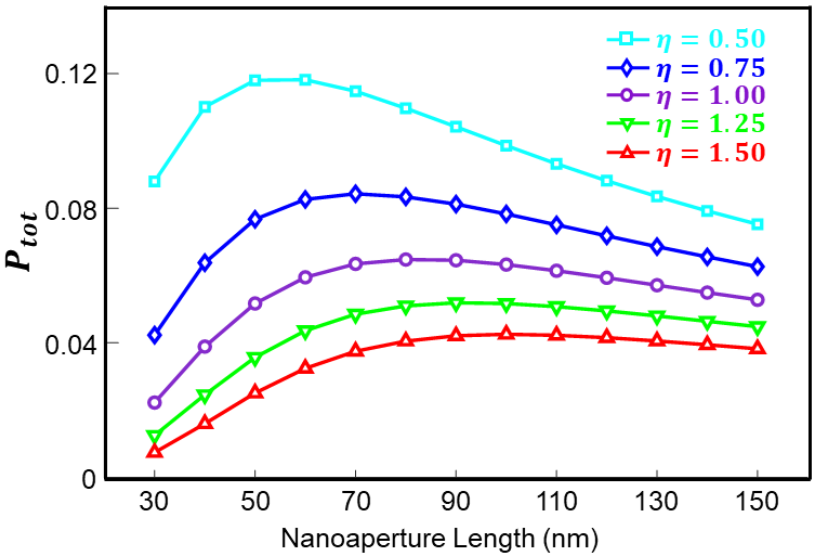

Figure S15. Total probability P_{tot} as a function of nanoaperture length for different dimensionless factors η. Cyan, blue, purple, green, and red curves correspond to $\eta = 0.5, 0.75, 1.0, 1.25$, and 1.5, respectively.

Supplementary References

1. Melhuish, W. H. Quantum efficiencies of fluorescence of organic substances: effect of solvent and concentration of the fluorescent solute1. *J. Phys. Chem.* **65**, 229–235 (1961).

2. Casalboni, M., De Matteis, F., Prosposito, P., Quatela, A.& Sarcinelli, F. Fluorescence efficiency of four infrared polymethine dyes. *Chem. Phys. Lett.* **373**, 372–378 (2003).

3. Ashkin, A. Optical trapping and manipulation of neutral particles using lasers. *Proc. Natl. Acad. Sci. USA* **94**, 4853–4860 (1997).

4. Jackson, J. D. Classical Electrodynamics (John Wiley & Sons, 2021).

5. Ashkin, A. Trapping of atoms by resonance radiation pressure. *Phys. Rev. Lett*. **40**, 729–732 (1978).